TITLE:

Emerging genetic diversity of SARS-CoV-2 RNA dependent RNA polymerase (RdRp) alters its B-cell epitopes.

AUTHORS:

Sushant Kumar[1] and Gajendra Kumar Azad[1#]

AFFALIATIONS:

[1]Department of Zoology, Patna University, Patna-800005, Bihar, India

[#]Corresponding Author: Gajendra Kumar Azad

Email address: gkazad@patnauniversity.ac.in

ABSTRACT

The RNA dependent RNA polymerase (RdRp) plays crucial role in virus life cycle by replicating the viral RNA genome. The SARS-CoV-2 is an RNA virus that rapidly spread worldwide and during this process acquired mutations. This study was carried out to identify mutations in RdRp as the SARS-CoV-2 spread in India. We compared the 668 RdRp sequences reported from India with the first reported RdRp sequence from Wuhan, China. Our data revealed that RdRp have acquired sixty mutations among Indian isolates. Our protein modelling study also revealed that several mutants including D833Y, A699S, Y149C and C464F can potentially alter stability and flexibility of RdRp. We also predicted the potential B cell epitopes contributed by RdRp and identified thirty-six linear continuous and twenty-five discontinuous epitopes. Among sixty RdRp mutants identified in this study, 40% of them localises in the B cell epitopes region. Altogether, this study highlights the need to identify and characterize the variations in RdRp to understand the impact of these mutations on SARS-CoV-2.

KEYWORDS: COVID-19; SARS-CoV-2; Mutations; B cell epitopes; RNA dependent RNA polymerase (RdRp); India

INTRODUCTION

SARS-CoV-2 genome encodes 29 protein molecules which are categorised into three groups including structural, non-structural and accessory proteins (Gordon et al., 2020). SARS-CoV-2 has four structural proteins namely Spike glycoprotein, Membrane protein, Envelope protein and Nucleocapsid Phosphoprotein (Wu et al., 2020). It also encodes sixteen non-structural proteins (Nsp1-16) and nine accessory proteins (Chan et al., 2020). The non-structural proteins are involved in the maintenance of its genome, virulence and important steps of virus life cycle. The 16 non-structural proteins are synthesised as a single polypeptide molecule of 7096 amino acids known as Orf1ab that is subsequently cleaved into 16 separate proteins (Chan et al., 2020). The RNA dependent RNA polymerase (RdRp), also known as Nsp12, is a non-structural protein that replicates SARS-CoV-2 RNA genome (Wu et al., 2020). It associates with Nsp7 and Nsp8 and exist as a trimeric complex inside the viral envelope structure (Peng et al., 2020). By itself, RdRp has a very weak polymerase activity; however, the complex of RdRp with Nsp7 and Nsp8 significantly increases RdRp processivity and template affinity (Te Velthuis et al., 2012; Zhai et al., 2005).

RdRp of SARS-CoV-2 is 932 residues in length and contains distinct polymerase and nucleotide binding domains with a central connecting domain (Gao et al., 2020). Structurally, RdRp is comprised of an N-terminal β-hairpin (residues 31-50) followed by an extended nidovirus RdRp-associated nucleotidyl-transferase domain (NiRAN, residues 115-250) (Yin et al., 2020). Following the NiRAN domain is an interface domain (residues 251-365) connected to the RdRp domain (residues 366-920). Further, the domains of RdRp arranges in such a way that it forms a canonical right-handed cup configuration (Mcdonald, 2013), with the finger subdomain (resides 397-581 and residues 621-679) forming a closed circle with the thumb subdomain (residues 819-920)(Yin et al., 2020).

The SARS-CoV-2 was first reported from Wuhan province China in late 2019 (Wu et al., 2020). Wet sea food market area of Wuhan reported patients with pneumonia like symptoms, which was later identified as SARS-CoV-2 because of its similarity with SARS-CoV (Gorbalenya et al., 2020). The SARS-CoV-2 is highly contagious and causes mild to severe respiratory distress in infected individuals and the disease has been named as COVID-19 (World Health Organization, 2020). The SARS-CoV-2 spread very fast and within few months reached almost all countries around the globe (Worldometers, 2020). As of 02nd May 2021, there are more than 150 million confirmed cases of COVID-19 and approximately 3 million deaths worldwide. This virus has caused global healthcare emergency because of its fast spread and sudden exponential rise in the COVID-19 patients and declared pandemic by world health organisation (WHO) (Cucinotta and Vanelli, 2020). This pandemic has caused enormous economic losses due to closure of most of the economic activities worldwide.

As the SARS-CoV-2 spread to other geographical areas with different climatic conditions compared to Wuhan, China, it started to mutate (Pachetti et al., 2020). The mutations acquired by the SARS-CoV-2 are retained as a consequence of natural selection, if the variants are more adaptable to the new conditions. In order to understand the variations occurring in RdRp among Indian geographical area, we analysed 668 RdRp sequences reported from India to identified sixty mutations. The B cell epitopes contributed by RdRp were predicted in silico, their functional consequences as well as the possible effect of mutations on them have been discussed.

MATERIAL AND METHODS

Protein Sequences retrieval from NCBI-virus-database

NCBI-virus-database is a repository for the nucleotide and protein sequences. This database also has protein sequences of SARS-CoV-2 that are available for users. We download the sequences of Orf1ab that contains all non-structural proteins including the RdRp sequence as described earlier (Azad, 2020). As of 10th April 2021, NCBI-virus-database has 668 sequences deposited from the Indian COVID-19 patients. The supplementary table 1 shows the list of protein identifier accession number used in this analysis. The RdRp is located from 4393 to 5324 residues in Orf1ab which corresponds to 932 amino acids in length. The RdRp reference or wild type sequence was also downloaded from NCBI virus database. The accession number of reference sequence used in this study is YP_009724389 which is the first reported sequence of SARS-CoV-2 from Wuhan, China (Wu et al., 2020).

Identification of RdRp mutants by multiple sequence alignments (MSAs)

In order to identify the variations present in the RdRp sequences among Indian isolates of SARS-CoV-2, the MSAs were conducted by Clustal omega programe (Madeira et al., 2019) as described earlier (Azad, 2021a). First, we uploaded the RdRp sequences in Clustal omega webserver and run the programe that uses HMM and pairwise alignment to generate the data. The variations from the reference sequence were properly marked and used for further analysis.

B cell epitope prediction

B cell prediction methods to predict Linear B cell epitopes based on sequence characteristics of the antigen using amino acid scales and HMMs. The prediction of linear continuous B cell epitopes were conducted by IEDB (Immune Epitope Database and Analysis Resource) (Vita et al., 2019). The IEDB is an online server tool which predicts epitopes by a prediction method known as ‘Bepipred linear epitope prediction method 2.0’. For this prediction the threshold value of 0.500 was used during the evaluation.

The prediction of discontinuous B cell epitopes was performed by an online tool 'DiscoTope 2.0'. For this prediction the threshold value was set at -3.7.

Protein modelling studies

We performed protein modelling studies to understand the variation observed in the secondary structure might have any consequences on the three-dimensional structure of protein. This analysis was performed by DynaMut programe (Rodrigues et al., 2018) as described earlier (Azad, 2021b). This server uses the solved crystal structure of proteins and predicts the effect of mutation on the stability, intramolecular interaction and molecular fluctuations in the protein structure. For this study, we used recently reported structure of RdRp (PDB ID: 7BV1)(Yin et al., 2020). The effect of mutations on protein is shown in terms of difference in free energy (ΔΔG). The positive value indicates stabilizing mutation; however, negative value represents destabilizing mutation. DynaMut provides difference in vibrational entropy (ΔΔSvib ENCOM) between the wild type and mutant protein. The positive ΔΔSvib ENCOM indicates increase in protein flexibility and negative ΔΔSvib ENCOM represents increase in rigidity of protein structure due to mutations. We ran DynaMut webserver to calculate the ΔΔG and ΔΔSvib ENCOM that provides the impact of mutation on protein structure and stability. DynaMut server also provides the visual representation of the intramolecular interactions contributed by wild type and mutant residues with the neighbouring residues.

RESULTS

RdRp is frequently mutated among Indian isolates of SARS-CoV-2

In order to identify the mutations in RdRp, we compared the first reported sequence of RdRp from Wuhan, China with the sequences reported from India. In this analysis, we used 668 RdRp sequences reported from India and performed Clustal Omega mediated multiple sequence alignment with an aim to identify variations in amino acids between the sequences. The RdRp polypeptide sequence reported from Wuhan, China was used as wild type sequence. Our data revealed sixty mutations present among the Indian sequences of RdRp as shown in table 1. The table also shows the location of each mutation in the RdRp polypeptide sequences and the effect of mutation on amino acid charge and polarity. The mutations are also demonstrated on the schematic representation of RdRp as shown in figure 1A and B. Our result show that the mutations are spreading all over the RdRp polypeptide sequence. The distribution of mutations in different domains of RdRp has been highlighted in figure 1B. Our MSA data strongly indicates that RdRp is one of the most

frequently mutated protein of SARS-CoV-2 because we observed sixty mutations in just 668 sequences analysed in this study.

Mutations affect RdRp protein dynamic stability and flexibility

We performed protein modelling studies using DynaMut programe to understand, if the mutation observed in RdRp can alter protein structural integrity. The DynaMut programe does protein modelling for those proteins whose crystal structure has been solved. For this protein modelling study, we used recently reported crystal structure of RdRp (PDB ID: 7BV1)(Yin et al., 2020). First, we calculated the differences in free energy (ΔΔG) between wild-type and mutant. Our data revealed that mutations at twenty-two positions cause stabilisation in protein structure (positive ΔΔG) as shown in table 2, maximum positive ΔΔG was obtained for D833Y (1.372 kcal/mol). Similarly, the mutations at twenty-eight positions cause destabilisation (negative ΔΔG) in protein structure upon mutation (Table 2), maximum negative ΔΔG was obtained for the mutant A699S (-2.233 kcal/mol).

Next, we measured the changes in vibrational entropy energy (ΔΔSVibENCoM) between the wild type and the mutant. The negative and positive ΔΔSVibENCoM values depict the rigidification and gain in protein flexibility upon mutation, respectively. Our data revealed that mutation at twenty-seven positions causes increase in flexibility of mutant protein (positive ΔΔSVibENCoM). The maximum positive ΔΔSVibENCoM was obtained for Y149C (1.065 kcal.mol-1.K-1) mutant. Similarly, the mutations at rest of the twenty-three positions cause rigidification of protein structure (negative ΔΔSVibENCoM) in protein structure upon mutation (Table 2). The maximum negative ΔΔSVibENCoM was obtained for C464F (-1.092 kcal.mol-1.K-1) mutant. Altogether, our data revealed that the mutation observed in RdRp affects both protein dynamicity and flexibility.

Identification of B cell epitopes of RdRp

The continuous B-cell epitopes of RdRp were predicted by IEDB webserver tool and the epitopes are shown in figure 2A. The yellow area of the graph corresponds to those regions of the RdRp that can potentially contribute to the B cell epitopes. Our data demonstrated thirty-six epitopes of varying lengths that could potentially act as B cell epitopes (figure 2B). Among those peptides, the ‘peptide 18’ is the largest epitopes, which is forty-four amino acid in length (from RdRp residue 482 to 525). Similarly, peptide 5, 19, 30, 31 and 34 are comprised of single amino acid only (figure 2B).

Subsequently, we predicted the B cell epitopes of RdRp based on its three dimensional structure using DiscoTope 2.0 webserver tool (Kringelum et al., 2012). Our analysis revealed twenty-five discontinuous epitopes of RdRp having high score. The locations of these epitopes are highlighted in figure 2C along with its propensity and DiscoTope score.

Among discontinuous epitopes, approximately 80% of them (20 out of 25) reside towards the C-terminal end of RdRp (from residue 800 to 932) as shown in figure 2C. Altogether, our data revealed B cell epitopes contributed by RdRp.

RdRp mutants preferentially localises in the B cell epitopes region

Subsequently, we analysed and compared the RdRp mutations that reside in the linear-continuous and discontinuous B cell epitopes. Our data revealed that out of 60 mutants observed in this study, 24 resides in the B cell epitope region of RdRp (figure 3A). These 24 mutants correspond to 40% of the total mutants observed among Indian isolates. The details of all 24 mutants that localises in B cell epitope region are shown in figure 3B. Altogether, our data strongly suggest that RdRp mutants preferentially localises in B cell epitope region.

DISCUSSION

The coronaviruses belongs to RNA viruses that exhibits high rate of mutations in their genome (Benvenuto et al., 2020). As these viruses spread to new locations they keep on acquiring mutations and few of them are naturally selected because of their beneficial effect on the virus. The SARS-CoV-2 was first reported from Wuhan, china and within a span of few months it spread to almost all countries worldwide (Worldometers, 2020). The researchers around the globe sequenced the SARS-CoV-2 to understand the genomic properties of this virus and soon identify various mutations. The investigation on the genomic variation acquired by SARS-CoV-2 is indispensable for understanding the epidemiology, pathogenesis; devise preventive measures and treatment strategies against COVID-19.

The earlier variation studies on SARS-CoV-2 revealed that RdRp is among the mutational hotspot protein (Pachetti et al., 2020). In the similar directions, this study was conducted with an aim to identify mutations in RdRp from Indian isolates. Our earlier study revealed seven crucial mutations in RdRp of SARS-CoV-2 (Chand et al., 2020) that can have potential impact on this protein function. The present study identifies and characterises B cell epitope contributed by RdRp and correlate them with the observed mutants. In this study, we analysed 668 RdRp sequences reported from India till April 2021 date and identified sixty mutations in RdRp. Our protein modelling studies revealed various interesting mutations including D833Y, A699S, Y149C and C464F (table 2) that can potentially affect stability and flexibility of RdRp. So far, we analysed 668 sequences from India and identified sixty mutations which indicates that RdRp is one of the mutational hotspot protein of SARS-CoV-2 in India. Furthermore, we did prediction study to identify B cell epitopes contributed by RdRp. Our data revealed that there are thirty-six high rank linear- continuous B cell epitope as well as twenty-five discontinuous B cell epitopes. Moreover, we also identified that out of sixty

mutants identified among Indian isolates, twenty-four resides (40%) in these B cell epitope region.

The variations in RdRp or any other protein of SARS-CoV-2 will possibly tell us how the virus is evolving. Earlier studies with RNA viruses have also shown that these viruses keep on mutating to better adapt and survive in the host (Sanjuán and Domingo-Calap, 2016). Here, in this study, we have reported RdRp mutations, its correlation with B cell epitopes. However, it warrants future studies to understand the possible effect of these mutations on virus infectivity and life cycle.

CONCLUSIONS

The pandemic caused by SARS-CoV-2 have adverse impact on health services worldwide with economic fallout of most of the countries. Understanding the genetic variations in SARS-CoV-2 will help to better devise the preventive and treatment strategies against this virus. Here, our data show various mutations in RdRp from India and their impact on B cell epitopes by *in silico* studies. Altogether, the data presented here could help scientific community to better understand the immunological aspect of SARS-CoV-2.

ACKNOWLEDGEMENTS

We would like to acknowledge Patna University, Patna, Bihar (India) for providing infrastructural support for this study.

REFERENCES

Azad, G.K., 2021a. The molecular assessment of SARS-CoV-2 Nucleocapsid Phosphoprotein variants among Indian isolates. Heliyon. https://doi.org/10.1016/j.heliyon.2021.e06167

Azad, G.K., 2021b. Identification and molecular characterization of mutations in nucleocapsid phosphoprotein of SARS-CoV-2. PeerJ. https://doi.org/10.7717/peerj.10666

Azad, G.K., 2020. Identification of novel mutations in the methyltransferase complex (Nsp10-Nsp16) of SARS-CoV-2. Biochem. Biophys. Reports. https://doi.org/10.1016/j.bbrep.2020.100833

Benvenuto, D., Giovanetti, M., Ciccozzi, A., Spoto, S., Angeletti, S., Ciccozzi, M., 2020. The 2019-new coronavirus epidemic: Evidence for virus evolution. J. Med. Virol. https://doi.org/10.1002/jmv.25688

Chan, J.F.W., Kok, K.H., Zhu, Z., Chu, H., To, K.K.W., Yuan, S., Yuen, K.Y., 2020. Genomic characterization of the 2019 novel human-pathogenic coronavirus isolated from a patient with atypical pneumonia after visiting Wuhan. Emerg. Microbes Infect.

296 https://doi.org/10.1080/22221751.2020.1719902
297 Chand, G.B., Banerjee, A., Azad, G.K., 2020. Identification of novel mutations in RNA-
298 dependent RNA polymerases of SARS-CoV-2 and their implications on its protein
299 structure. PeerJ 8, e9492. https://doi.org/10.7717/peerj.9492
300 Cucinotta, D., Vanelli, M., 2020. WHO declares COVID-19 a pandemic. Acta Biomed.
301 https://doi.org/10.23750/abm.v91i1.9397
302 Gao, Y., Yan, L., Huang, Y., Liu, F., Zhao, Y., Cao, L., Wang, T., Sun, Q., Ming, Z., Zhang,
303 L., Ge, J., Zheng, L., Zhang, Y., Wang, H., Zhu, Y., Zhu, C., Hu, T., Hua, T., Zhang, B.,
304 Yang, X., Li, J., Yang, H., Liu, Z., Xu, W., Guddat, L.W., Wang, Q., Lou, Z., Rao, Z.,
305 2020. Structure of the RNA-dependent RNA polymerase from COVID-19 virus. Science
306 (80-.). https://doi.org/10.1126/science.abb7498
307 Gorbalenya, A.E., Baker, S.C., Baric, R.S., de Groot, R.J., Drosten, C., Gulyaeva, A.A.,
308 Haagmans, B.L., Lauber, C., Leontovich, A.M., Neuman, B.W., Penzar, D., Perlman, S.,
309 Poon, L.L.M., Samborskiy, D. V., Sidorov, I.A., Sola, I., Ziebuhr, J., 2020. The species
310 Severe acute respiratory syndrome-related coronavirus: classifying 2019-nCoV and
311 naming it SARS-CoV-2. Nat. Microbiol. https://doi.org/10.1038/s41564-020-0695-z
312 Gordon, D.E., Jang, G.M., Bouhaddou, M., Xu, J., Obernier, K., White, K.M., O'Meara, M.J.,
313 Rezelj, V. V., Guo, J.Z., Swaney, D.L., Tummino, T.A., Huettenhain, R., Kaake, R.M.,
314 Richards, A.L., Tutuncuoglu, B., Foussard, H., Batra, J., Haas, K., Modak, M., Kim, M.,
315 Haas, P., Polacco, B.J., Braberg, H., Fabius, J.M., Eckhardt, M., Soucheray, M.,
316 Bennett, M.J., Cakir, M., McGregor, M.J., Li, Q., Meyer, B., Roesch, F., Vallet, T., Mac
317 Kain, A., Miorin, L., Moreno, E., Naing, Z.Z.C., Zhou, Y., Peng, S., Shi, Y., Zhang, Z.,
318 Shen, W., Kirby, I.T., Melnyk, J.E., Chorba, J.S., Lou, K., Dai, S.A., Barrio-Hernandez,
319 I., Memon, D., Hernandez-Armenta, C., Lyu, J., Mathy, C.J.P., Perica, T., Pilla, K.B.,
320 Ganesan, S.J., Saltzberg, D.J., Rakesh, R., Liu, X., Rosenthal, S.B., Calviello, L.,
321 Venkataramanan, S., Liboy-Lugo, J., Lin, Y., Huang, X.P., Liu, Y.F., Wankowicz, S.A.,
322 Bohn, M., Safari, M., Ugur, F.S., Koh, C., Savar, N.S., Tran, Q.D., Shengjuler, D.,
323 Fletcher, S.J., O'Neal, M.C., Cai, Y., Chang, J.C.J., Broadhurst, D.J., Klippsten, S.,
324 Sharp, P.P., Wenzell, N.A., Kuzuoglu, D., Wang, H.Y., Trenker, R., Young, J.M.,
325 Cavero, D.A., Hiatt, J., Roth, T.L., Rathore, U., Subramanian, A., Noack, J., Hubert, M.,
326 Stroud, R.M., Frankel, A.D., Rosenberg, O.S., Verba, K.A., Agard, D.A., Ott, M.,
327 Emerman, M., Jura, N., von Zastrow, M., Verdin, E., Ashworth, A., Schwartz, O.,
328 d'Enfert, C., Mukherjee, S., Jacobson, M., Malik, H.S., Fujimori, D.G., Ideker, T., Craik,
329 C.S., Floor, S.N., Fraser, J.S., Gross, J.D., Sali, A., Roth, B.L., Ruggero, D., Taunton,
330 J., Kortemme, T., Beltrao, P., Vignuzzi, M., García-Sastre, A., Shokat, K.M., Shoichet,
331 B.K., Krogan, N.J., 2020. A SARS-CoV-2 protein interaction map reveals targets for
332 drug repurposing. Nature. https://doi.org/10.1038/s41586-020-2286-9

Kringelum, J.V., Lundegaard, C., Lund, O., Nielsen, M., 2012. Reliable B Cell Epitope Predictions: Impacts of Method Development and Improved Benchmarking. PLoS Comput. Biol. https://doi.org/10.1371/journal.pcbi.1002829

Madeira, F., Park, Y.M., Lee, J., Buso, N., Gur, T., Madhusoodanan, N., Basutkar, P., Tivey, A.R.N., Potter, S.C., Finn, R.D., Lopez, R., 2019. The EMBL-EBI search and sequence analysis tools APIs in 2019. Nucleic Acids Res. https://doi.org/10.1093/nar/gkz268

Mcdonald, S.M., 2013. RNA synthetic mechanisms employed by diverse families of RNA viruses. Wiley Interdiscip. Rev. RNA. https://doi.org/10.1002/wrna.1164

Pachetti, M., Marini, B., Benedetti, F., Giudici, F., Mauro, E., Storici, P., Masciovecchio, C., Angeletti, S., Ciccozzi, M., Gallo, R.C., Zella, D., Ippodrino, R., 2020. Emerging SARS-CoV-2 mutation hot spots include a novel RNA-dependent-RNA polymerase variant. J. Transl. Med. https://doi.org/10.1186/s12967-020-02344-6

Peng, Q., Peng, R., Yuan, B., Zhao, J., Wang, M., Wang, X., Wang, Q., Sun, Y., Fan, Z., Qi, J., Gao, G.F., Shi, Y., 2020. Structural and biochemical characterization of nsp12-nsp7-nsp8 core polymerase complex from SARS-CoV-2. Cell Rep. https://doi.org/10.1016/j.celrep.2020.107774

Rodrigues, C.H.M., Pires, D.E.V., Ascher, D.B., 2018. DynaMut: Predicting the impact of mutations on protein conformation, flexibility and stability. Nucleic Acids Res. https://doi.org/10.1093/nar/gky300

Sanjuán, R., Domingo-Calap, P., 2016. Mechanisms of viral mutation. Cell. Mol. Life Sci. https://doi.org/10.1007/s00018-016-2299-6

Te Velthuis, A.J.W., Van Den Worm, S.H.E., Snijder, E.J., 2012. The SARS-coronavirus nsp7+nsp8 complex is a unique multimeric RNA polymerase capable of both de novo initiation and primer extension. Nucleic Acids Res. https://doi.org/10.1093/nar/gkr893

Vita, R., Mahajan, S., Overton, J.A., Dhanda, S.K., Martini, S., Cantrell, J.R., Wheeler, D.K., Sette, A., Peters, B., 2019. The Immune Epitope Database (IEDB): 2018 update. Nucleic Acids Res. https://doi.org/10.1093/nar/gky1006

World Health Organization, 2020. Naming the coronavirus disease (COVID-19) and the virus that causes it. World Heal. Organ.

Worldometers, 2020. COVID-19 CORONAVIRUS PANDEMIC [WWW Document]. Worldometers. https://doi.org/-

Wu, F., Zhao, S., Yu, B., Chen, Y.M., Wang, W., Song, Z.G., Hu, Y., Tao, Z.W., Tian, J.H., Pei, Y.Y., Yuan, M.L., Zhang, Y.L., Dai, F.H., Liu, Y., Wang, Q.M., Zheng, J.J., Xu, L., Holmes, E.C., Zhang, Y.Z., 2020. A new coronavirus associated with human respiratory disease in China. Nature. https://doi.org/10.1038/s41586-020-2008-3

Yin, W., Mao, C., Luan, X., Shen, D.-D., Shen, Q., Su, H., Wang, X., Zhou, F., Zhao, W., Gao, M., Chang, S., Xie, Y.-C., Tian, G., Jiang, H.-W., Tao, S.-C., Shen, J., Jiang, Y.,

Jiang, H., Xu, Y., Zhang, S., Zhang, Y., Xu, H.E., 2020. Structural basis for inhibition of the RNA-dependent RNA polymerase from SARS-CoV-2 by remdesivir. Science (80-.). https://doi.org/10.1126/science.abc1560

Zhai, Y., Sun, F., Li, X., Pang, H., Xu, X., Bartlam, M., Rao, Z., 2005. Insights into SARS-CoV transcription and replication from the structure of the nsp7-nsp8 hexadecamer. Nat. Struct. Mol. Biol. https://doi.org/10.1038/nsmb999

TABLE AND FIGURE LEGENDS

Table 1. The list demonstrates the location and details of mutations of RdRp identified by Clustal Omega multiple sequence alignments. The RdRp sequence reported from Wuhan, China was used as wild type sequence for this analysis. The 668 sequences of RdRp reported from India were used for identifying mutations.

S. No.	Wild-type	Charge Changes	Polarity Changes
1	K59N	Basic to Neutral	P to P
2	T85I	Neutral to Neutral	P to NP
3	K91N	Basic to Neutral	P to P
4	P94S	Neutral to Neutral	NP to P
5	A95V	Neutral to Neutral	NP to P
6	A97V	Neutral to Neutral	NP to P
7	I101L	Neutral to Neutral	NP to NP
8	M110K	Neutral to Basic	NP to P
9	R118C	Basic to Neutral	P to P
10	Y122F	Neutral to Neutral	P to NP
11	D140G	Acidic to Neutral	P to NP
12	T141I	Neutral to Neutral	P to NP
13	E144K	Acidic to Basic	P to P
14	T148I	Neutral to Neutral	P to NP
15	Y149C	Neutral to Neutral	P to P
16	R173H	Basic to Basic	P to P
17	A185V	Neutral to Neutral	NP to NP
18	M196I	Neutral to Neutral	NP to NP
19	I201L	Neutral to Neutral	NP to NP
20	T248I	Neutral to Neutral	P to NP
21	D269N	Acidic to Neutral	P to P
22	E278D	Acidic to Acidic	P to P
23	D284Y	Acidic to Neutral	P to P
24	T293I	Neutral to Neutral	P to NP
25	H295Y	Basic to Neutral	P to P
26	P323L	Neutral to Neutral	NP to NP

27	L329I	Neutral to Neutral	NP to NP
28	V342A	Neutral to Neutral	P to NP
29	V342L	Neutral to Neutral	NP to NP
30	V354A	Neutral to Neutral	P to NP
31	V354L	Neutral to Neutral	NP to NP
32	V398L	Neutral to Neutral	NP to NP
33	A406V	Neutral to Neutral	NP to NP
34	M463I	Neutral to Neutral	NP to NP
35	C464F	Acidic to Neutral	P to NP
36	I488S	Neutral to Neutral	NP to P
37	A526V	Neutral to Neutral	NP to NP
38	I536T	Neutral to Neutral	NP to P
39	V605A	Neutral to Neutral	NP to NP
40	M608I	Neutral to Neutral	NP to NP
41	L638F	Neutral to Neutral	NP to NP
42	T643I	Neutral to Neutral	P to NP
43	T644M	Neutral to Neutral	P to NP
44	S647I	Neutral to Neutral	P to NP
45	M668I	Neutral to Neutral	NP to NP
46	A699S	Neutral to Neutral	NP to P
47	L775P	Neutral to Neutral	NP to NP
48	E802A	Acidic to Neutral	P to NP
49	S814P	Neutral to Neutral	P to NP
50	Q822H	Neutral to Basic	P to P
51	D833Y	Acidic to Neutral	P to P
52	T848I	Neutral to Neutral	P to NP
53	S853L	Neutral to Neutral	P to NP
54	V880I	Neutral to Neutral	NP to NP
55	D893Y	Acidic to Neutral	P to P
56	Y908I	Neutral to Neutral	P to NP
57	T909I	Neutral to Neutral	P to NP
58	S913L	Neutral to Neutral	P to NP
59	S919L	Neutral to Neutral	P to NP
60	P925S	Neutral to Neutral	NP to P

384

385 Table 2. The ΔΔG and ΔΔSvib ENCOM values obtained by protein modelling using DynaMut
386 programe. The positive and negative ΔΔG represents increase and decrease in protein
387 stability upon mutation. Similarly, the positive and negative ΔΔSvib ENCOM represents the
388 increase in flexibility and rigidity upon mutations.

389

S. No.	Mutation	ΔΔG (kcal/mol)	ΔΔSVib ENCoM (kcal.mol-1.K-1)
1	T85I	-0.707	-0.074
2	K91N	-0.311	0.295

3	P94S	-0.035	-0.131
4	A95V	-0.669	-0.627
5	A97V	0.469	-1.020
6	R118C	0.005	0.055
7	Y122F	0.225	0.273
8	D140G	-0.18	0.035
9	T141I	1.041	-0.231
10	E144K	-0.236	0.353
11	T148I	1.156	-0.098
12	Y149C	0.237	1.065
13	R173H	-0.284	0.01
14	A185V	-0.179	-0.369
15	M196I	-0.554	0.094
16	I201L	0.105	0.057
17	T248I	0.452	-0.08
18	D269N	-0.362	0.08
19	E278D	-0.714	0.103
20	D284Y	0.346	-0.459
21	T293I	0.264	-0.016
22	H295Y	0.304	0.141
23	P323L	0.53	-0.252
24	L329I	0.081	0.231
25	V342A	-0.454	0.402
26	V342L	1.027	-0.025
27	V354A	-1.811	0.277
28	V354L	-0.162	-0.387
29	V398L	0.37	0.031
30	A406V	-0.148	-0.047
31	M463I	0.483	0.25
32	C464F	1.251	-1.092
33	I488S	-1.617	0.205
34	A526V	0.305	-0.109
35	I536T	-1.703	0.348
36	V605A	-1.528	0.596
37	L638F	-0.167	-0.297
38	T643I	-0.383	-0.074
39	T644M	-0.084	-0.037
40	S647I	-0.272	0.166
41	M668I	0.104	0.066
42	A699S	-2.233	-0.185
43	L775P	-0.6	0.754
44	E802A	-0.835	0.49
45	S814P	-0.083	0.113
46	Q822H	0.006	0.514

47	D833Y	1.372	-0.397
48	V880I	-0.087	-0.146
49	D893Y	0.088	-0.168
50	S913L	-0.116	0.012

Figure 1: The details of the mutation identified in RdRp among Indian SARS-CoV-2 isolates. A) Schematic diagram of the domain architecture of RdRp. Each domain of RdRp is represented by a unique color. The interdomain borders are labeled with residue numbers. B) The mutations present in RdRp among the Indian isolates of SARS-CoV-2 are demonstrated in the schematics.

Figure 2: Prediction of B-cell epitopes of RdRp. A) Linear continuous B-cell epitopes contributed by RdRp, the Y-axis of the graph corresponds to BepiPred score, while the X-axis depicts the RdRp residue positions in the sequence. The data was generated by IEDB webserver using 'Bepipred Linear Epitope Prediction 2.0' method. The chart is divided into two parts yellow and green. The RdRp residues present in the yellow have higher probability to be part of the linear continuous B cell epitope. B) The details of the linear continuous B cell epitopes are listed. The sequence of each peptide along with its start and end point in the RdRp polypeptide sequence is also mentioned. C) Prediction of discontinuous B-cell epitopes of RdRp by DiscoTope 2.0 web tool. The position of each predicted epitope is mentioned along with its propensity and DiscoTope score.

Figure 3: Correlation of RdRp mutants and B cell epitopes. A) the graph shows the distribution of RdRp mutants observed among Indian SARS-CoV-2 isolates. Out of 60, 24 mutants localises in B cell epitope region of RdRp. B) Detail of the RdRp mutants that localises in B cell epitope region.

Supplementary Table 1: List of protein identifier accession number used in this analysis. The sequences of each protein can be downloaded from NCBI-Virus-Database using the accession number provided in the list.

YP_009724389	QOS50986.1	QNL90834.1	QLI49743.1	QKY60095.1	QKJ84977.1	QJX44644.1
QTV76173.1	QOS51010.1	QNL90846.1	QLI49755.1	QKY60107.1	QKG91164.1	QJX44656.1
QTP17383.1	QOS51022.1	QNL90858.1	QLI49767.1	QKY60119.1	QKG91176.1	QJX44668.1
QTH36343.1	QOS51058.1	QNL90870.1	QLI49779.1	QKY60131.1	QKG91188.1	QJX44680.1
QTH36355.1	QOS51070.1	QNL90882.1	QLI49791.1	QKY60163.1	QKG91200.1	QJW39842.1
QTH36367.1	QOS51082.1	QNL90894.1	QLI49803.1	QKY60175.1	QKG91212.1	QJW39854.1
QTH36379.1	QOS51094.1	QNL90906.1	QLI49815.1	QKY60187.1	QKG91224.1	QJW39866.1
QTH36391.1	QOS51106.1	QNL90918.1	QLI52055.1	QKY60199.1	QKG91236.1	QJW39878.1
QTH36403.1	QOS51118.1	QNL98443.1	QLI52067.1	QKY60211.1	QKG91248.1	QJW39890.1

QTH36415.1	QOR63432.1	QNL98455.1	QLH64777.1	QKY60223.1	QKG91260.1	QJW39902.1
QTH36427.1	QOR63444.1	QNL98467.1	QLH64789.1	QKY60235.1	QKG91272.1	QJW39914.1
QTH36439.1	QOR63456.1	QNL98479.1	QLH64801.1	QKY60262.1	QKG91284.1	QJW39926.1
QTH36451.1	QOR63468.1	QNL35816.1	QLH64813.1	QKY64328.1	QKH78808.1	QJW69137.1
QTH36723.1	QOR63480.1	QNL35828.1	QLH64825.1	QKY64344.1	QKH78820.1	QJU70555.1
QTG68689.1	QOR63504.1	QNL35840.1	QLH64837.1	QKY64358.1	QKI10470.1	QJT43414.1
QTG68602.1	QOR64231.1	QNL35852.1	QLH64849.1	QKY64612.1	QKI28575.1	QJT43426.1
QTG68615.1	QOR64243.1	QNL35864.1	QLH64861.1	QKY64638.1	QKI28587.1	QJT43438.1
QTG40603.1	QOQ57010.1	QNL35876.1	QLH64875.1	QKY64790.1	QKI28599.1	QJT43450.1
QRY06669.1	QOQ57022.1	QNL35888.1	QLH64887.1	QKY65275.1	QKI28611.1	QJT43462.1
QRQ47003.1	QOQ57034.1	QNL35900.1	QLH64899.1	QKV25883.1	QKI28623.1	QJT43474.1
QRQ47018.1	QOQ57046.1	QNL35912.1	QLH64915.1	QKV25895.1	QKI28635.1	QJT43486.1
QRQ47032.1	QOQ57058.1	QNL35924.1	QLH64927.1	QKV25907.1	QKI28647.1	QJT43498.1
QRQ47071.1	QOQ57070.1	QNL35936.1	QLH64939.1	QKV25919.1	QKI28659.1	QJT43510.1
QRQ47083.1	QOQ57082.1	QNL35948.1	QLH90040.1	QKV25931.1	QKI28671.1	QJT43522.1
QRQ69195.1	QOQ57094.1	QNL35960.1	QLH90076.1	QKV25943.1	QKI28683.1	QJT43534.1
QRQ69279.1	QOQ57106.1	QNL35972.1	QLH90088.1	QKV25955.1	QKE61658.1	QJT43546.1
QRN68229.1	QOQ57119.1	QNL35984.1	QLH90101.1	QKV25967.1	QKE61670.1	QJT43558.1
QRN68241.1	QOQ72542.1	QNL35996.1	QLH93117.1	QKV25979.1	QKE61682.1	QJT43570.1
QRN68253.1	QOQ72554.1	QNL36008.1	QLH93129.1	QKV25991.1	QKE61694.1	QJT43582.1
QRN68266.1	QOQ72566.1	QNL36560.1	QLH93185.1	QKV26003.1	QKE61706.1	QJT43594.1
QRN68278.1	QOQ72578.1	QLY82444.1	QLH93199.1	QKV26015.1	QKE61718.1	QJT43606.1
QRN68302.1	QOQ84793.1	QLY82482.1	QLH93212.1	QKV26027.1	QKE61730.1	QJT43618.1
QRN68400.1	QOQ84824.1	QLY82500.1	QLH93283.1	QKV26039.1	QKE61742.1	QJT43630.1
QRN68424.1	QKM77202.1	QLY82512.1	QLF97937.1	QKV26051.1	QKE61754.1	QJT43642.1
QRN68442.1	QKM77214.1	QMC85346.1	QLF97949.1	QKV26063.1	QKE61766.1	QJT43654.1
QRM36235.1	QKM77226.1	QLQ87394.1	QLF97985.1	QKV26075.1	QKE61778.1	QJT43666.1
QRM91443.1	QKM77238.1	QLQ87406.1	QLF97997.1	QKV26087.1	QKE61790.1	QJT43678.1
QRE02629.2	QKM77250.1	QLQ87418.1	QLF98069.1	QKV27549.1	QKE61802.1	QJT43690.1
QRC50281.1	QKM77262.1	QLQ87430.1	QLF98081.1	QKV27561.1	QJY77053.1	QJT43702.1
QRC50293.1	QKM77274.1	QLQ87442.1	QLF98093.1	QKV27573.1	QJY51262.1	QJT43714.1
QRC50305.1	QNO30921.1	QLQ87454.1	QLF98105.1	QKV27585.1	QJY51274.1	QJT43726.1
QRC50340.1	QNO30933.1	QLQ87466.1	QLF98117.1	QKQ29884.1	QJY51286.1	QJS39637.1
QRC50364.1	QNN87972.1	QLQ87478.1	QLF98129.1	QKQ29944.1	QJY51346.1	QJS39649.1
QRC50492.1	QNN87984.1	QLQ87490.1	QLF98141.1	QKQ29956.1	QJY51358.1	QJR84343.1
QQJ94103.1	QNN87996.1	QLQ87502.1	QLF98153.1	QKQ29968.1	QJY51370.1	QJR84367.1
QQJ95306.1	QNN88008.1	QLQ87514.1	QLF98165.1	QKQ30028.1	QJY51382.1	QJR84379.1
QQH18637.1	QNN88020.1	QLQ87526.1	QLF98178.1	QKQ30040.1	QJY40383.1	QJR84391.1
QPZ33508.1	QNN88068.1	QLQ87550.1	QLF98198.1	QKQ30052.1	QJY40395.1	QJR84415.1
QPB40017.1	QNN88080.1	QLQ87574.1	QLF98210.1	QKQ30064.1	QJY40407.1	QJR84427.1
QPB40029.1	QNN88092.1	QLQ87598.1	QLF98222.1	QKQ30076.1	QJY40419.1	QJR84439.1
QPB40041.1	QNN88104.1	QLQ87610.1	QLF98234.1	QKQ30088.1	QJY40431.1	QJR84451.1
QPB40053.1	QNN88116.1	QLQ87622.1	QLF98246.1	QKQ30100.1	QJY40443.1	QJR84463.1
QPB40065.1	QNN88128.1	QLQ87634.1	QLF98258.1	QKQ30112.1	QJY40455.1	QJR84475.1
QPB40077.1	QNN88140.1	QLQ87658.1	QLF98275.1	QKQ30124.1	QJY40467.1	QJR84487.1
QPB40089.1	QNN88152.1	QLQ87682.1	QLF98287.1	QKQ30136.1	QJY40479.1	QJR84499.1

QPB40101.1	QNN88164.1	QLQ87694.1	QLA09686.1	QKQ30148.1	QJY40491.1	QJR84511.1
QPB40113.1	QNN88176.1	QLQ87706.1	QLA09698.1	QKQ30160.1	QJY40503.1	QJR84523.1
QPB40563.1	QNN88188.1	QLQ87718.1	QLA09710.1	QKQ30172.1	QJY40515.1	QJR84535.1
QPB40575.1	QNN88200.1	QLQ87730.1	QLA09722.1	QKQ30184.1	QJY40527.1	QJQ28343.1
QPB17918.1	QNN88212.1	QLQ87795.1	QLA09734.1	QKQ30196.1	QJY40539.1	QJQ28355.1
QPB17990.1	QNN88224.1	QLQ87983.1	QLA09746.1	QKQ30208.1	QJY40551.1	QJQ28367.1
QPB18014.1	QNN88236.1	QLQ87995.1	QLA09758.1	QKQ30220.1	QJY40563.1	QJQ28379.1
QPB18026.1	QNN88248.1	QLQ88046.1	QLA09770.1	QKQ30232.1	QJY40575.1	QJQ28391.1
QPB18050.1	QNN88260.1	QLQ88063.1	QLA09782.1	QKQ30244.1	QJY40587.1	QJQ28403.1
QPB18062.1	QNN88272.1	QLQ88075.1	QLA09794.1	QKQ30256.1	QJY40599.1	QJQ28415.1
QPB18074.1	QNN88284.1	QLQ88087.1	QLA09808.1	QKQ30268.1	QJW00289.1	QJQ28427.1
QPB18086.1	QNN88296.1	QLQ88102.1	QLA09820.1	QKQ63386.1	QJW00301.1	QJH92165.1
QPB18098.1	QNN88551.1	QLR06736.1	QLA09832.1	QKO00484.1	QJW00313.1	QJH92177.1
QPB18110.1	QNN88563.1	QLR06757.1	QLA09844.1	QKJ68410.1	QJW00325.1	QJF77844.1
QPB18122.1	QNN88575.1	QLR06769.1	QLA09856.1	QKJ68422.1	QJW00337.1	QJF77856.1
QPB18134.1	QNN88630.1	QLR06870.1	QLA09880.1	QKJ68434.1	QJW00349.1	QJF77868.1
QPB18158.1	QNN88642.1	QLR06882.1	QLA09904.1	QKJ68446.1	QJW00361.1	QJF77880.1
QPB18194.1	QNN88654.1	QLR06894.1	QLA10066.1	QKJ68458.1	QJW00373.1	QJC19489.1
QPB18206.1	QNN90122.1	QLR07146.1	QLA10078.1	QKJ68471.1	QJW00385.1	QHS34545.1
QPB39980.1	QNN90135.1	QLR07158.1	QLA10090.1	QKJ68483.1	QJW00397.1	QIA98582.1
QPB39992.1	QNN93013.1	QLR07170.1	QLA10102.1	QKJ68495.1	QJW00409.1	
QPB40004.1	QNN26334.1	QLR07182.1	QLA10114.1	QKJ68507.1	QJW00421.1	
QPA18453.1	QNN26346.1	QLR07194.1	QLA10126.1	QKJ68519.1	QJW00433.1	
QPA18457.1	QNN26358.1	QLR07206.1	QLA10138.1	QKJ68531.1	QJW00445.1	
QOW08181.2	QNN26370.1	QLR12235.1	QLA10150.1	QKJ68543.1	QJW00457.1	
QOU99168.1	QNN26382.1	QLR12247.1	QLA10162.1	QKJ68555.1	QJX44380.1	
QOU99261.1	QNN26394.1	QLR12259.1	QLA10174.1	QKJ68567.1	QJX44392.1	
QOU99272.1	QNN26406.1	QLR12271.1	QLA10186.1	QKJ68579.1	QJX44404.1	
QOU99283.1	QNN26418.1	QLR12283.1	QLA10198.1	QKJ68591.1	QJX44416.1	
QOU99294.1	QNN26430.1	QLR12295.1	QLA10210.1	QKJ68603.1	QJX44428.1	
QOS50509.1	QNN26442.1	QLR12307.1	QLA10222.1	QKJ68615.1	QJX44440.1	
QOS50580.1	QNN26454.1	QLR12319.1	QKY74626.1	QKJ68627.1	QJX44464.1	
QOS50592.1	QNN26466.1	QLR12331.1	QKY74638.1	QKJ68639.1	QJX44476.1	
QOS50604.1	QNN26478.1	QLR12343.1	QKY59939.1	QKJ68651.1	QJX44500.1	
QOS50616.1	QNN30834.1	QLR12355.1	QKY59951.1	QKJ68663.1	QJX44512.1	
QOS50628.1	QNN30858.1	QLR12415.1	QKY59963.1	QKJ68675.1	QJX44536.1	
QOS50676.1	QNN30870.1	QLR12438.1	QKY59975.1	QKJ68687.1	QJX44548.1	
QOS50712.1	QNN31194.1	QLR60574.1	QKY59987.1	QKJ68699.1	QJX44560.1	
QOS50879.1	QNN31206.1	QLR80398.1	QKY59999.1	QKJ68711.1	QJX44572.1	
QOS50891.1	QNN81330.1	QLS04049.1	QKY60023.1	QKJ68723.1	QJX44584.1	
QOS50926.1	QNN81490.1	QLI49695.1	QKY60047.1	QKJ68735.1	QJX44596.1	
QOS50938.1	QNN81502.1	QLI49707.1	QKY60059.1	QKJ84941.1	QJX44608.1	
QOS50950.1	QNN83660.1	QLI49719.1	QKY60071.1	QKJ84953.1	QJX44620.1	
QOS50962.1	QNN83672.1	QLI49731.1	QKY60083.1	QKJ84965.1	QJX44632.1	

416

417

418

Figure 1

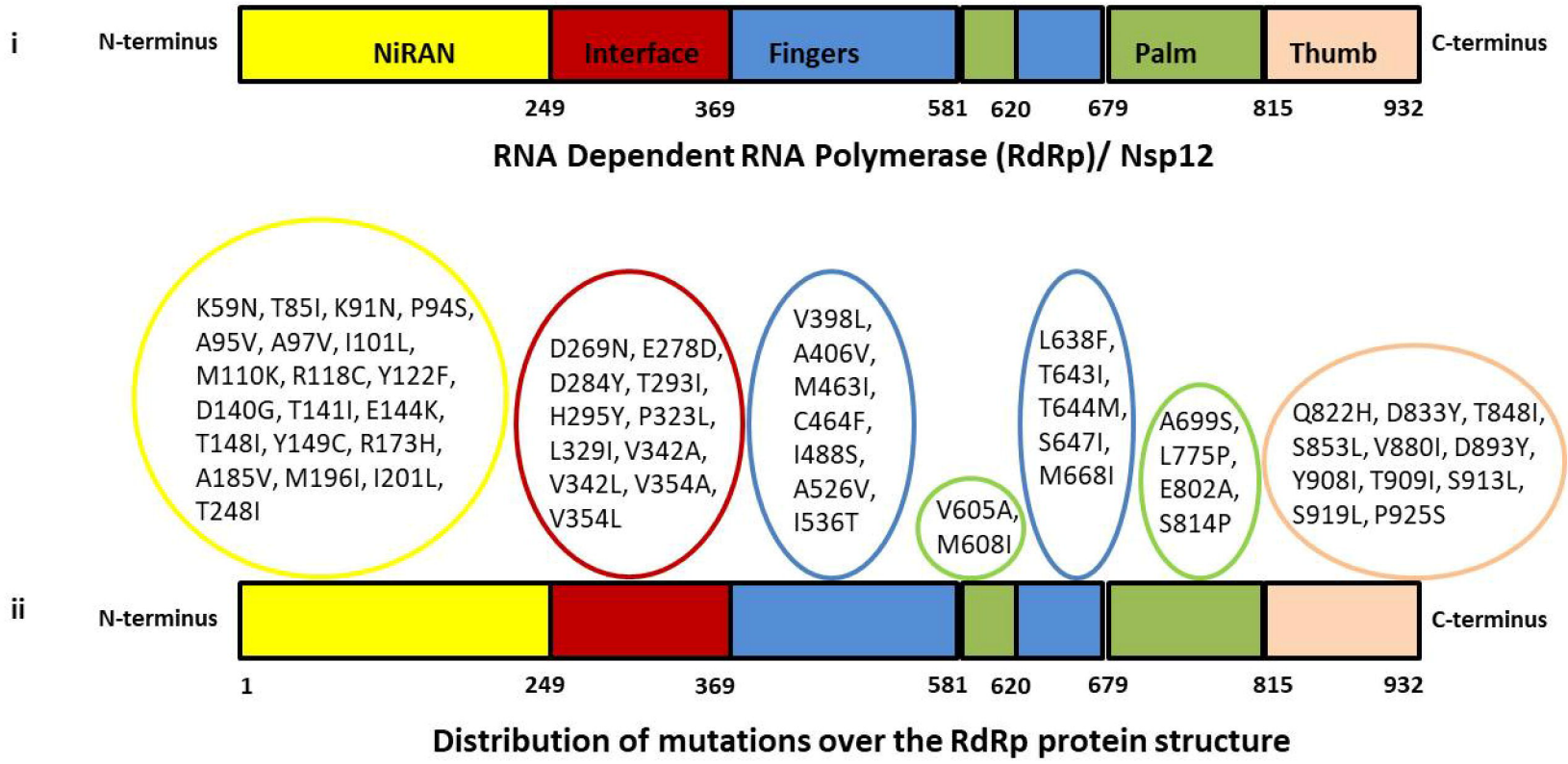
i
N-terminus
NiRAN
Interface
Fingers
Palm
Thumb
C-terminus
249
369
581
620
679
815
932
RNA Dependent RNA Polymerase (RdRp)/ Nsp12
K59N, T85I, K91N, P94S, A95V, A97V, I101L, M110K, R118C, Y122F, D140G, T141I, E144K, T148I, Y149C, R173H, A185V, M196I, I201L, T248I
D269N, E278D, D284Y, T293I, H295Y, P323L, L329I, V342A, V342L, V354A, V354L
V398L, A406V, M463I, C464F, I488S, A526V, I536T
V605A, M608I
L638F, T643I, T644M, S647I, M668I
A699S, L775P, E802A, S814P
Q822H, D833Y, T848I, S853L, V880I, D893Y, Y908I, T909I, S913L, S919L, P925S
ii
N-terminus
C-terminus
1
249
369
581
620
679
815
932
Distribution of mutations over the RdRp protein structure

Figure 2

A

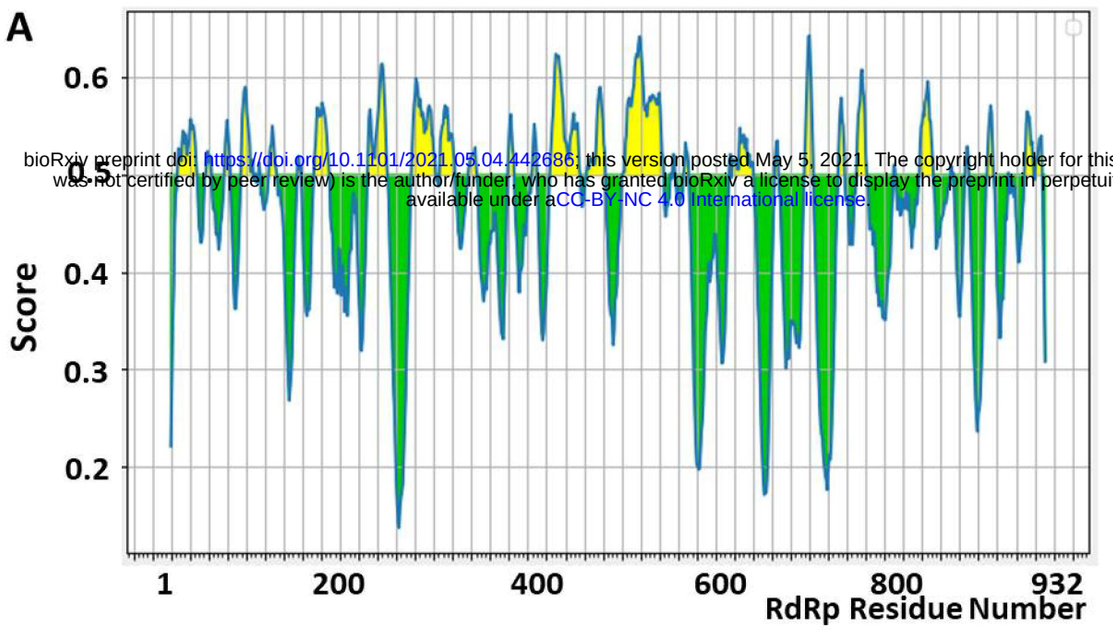

B

Linear- continuous B cell epitopes RdRp

Epitopes	Peptide Start	Peptide End	Peptide Sequence
Peptide 1	8	28	LNRVCGVSAARLTPCGTGTST
Peptide 2	39	44	NDKVAG
Peptide 3	58	64	EKDEDDN
Peptide 4	76	88	TFSNYQHEETIYN
Peptide 5	91	91	K
Peptide 6	95	96	AV
Peptide 7	106	113	IDGDMVPH
Peptide 8	136	139	EGNC
Peptide 9	154	169	DDYFNKKDWYDFVENP
Peptide 10	211	231	DLNGNWYDFGDFIQTTPGSGV
Peptide 11	257	283	VDTDLTKPYIKWDLLKYDFTEERLKLF
Peptide 12	288	303	KYWDQTYHPNCVNCLD
Peptide 13	318	326	STVFPPTSF
Peptide 14	360	366	NLHSSRL
Peptide 15	386	390	NLLLD
Peptide 16	405	436	VAFQTVKPGNFNKDFYDFAVSKGFFKEGSSVE
Peptide 17	444	463	QDGNAAISDYDYYRYNLPTM
Peptide 18	482	525	CYDGGCINANQVIVNNLDKSAGFPFNKWGKA RLYYDSMSYEDQD
Peptide 19	533	533	R
Peptide 20	536	537	IP
Peptide 21	547	552	AISAKN
Peptide 22	596	597	GG
Peptide 23	599	621	HNMLKTVYSDVENPHLMGWDYPK
Peptide 24	644	648	TCCSL
Peptide 25	676	685	KPGGTSSGDA
Peptide 26	712	718	GNKIADK
Peptide 27	731	742	LYRNRDVDTDFV
Peptide 28	771	772	AS
Peptide 29	798	812	KCWTETDLTKGPHEF
Peptide 30	832	832	P
Peptide 31	834	834	P
Peptide 32	847	850	IVKT
Peptide 33	871	877	KHPNQEY
Peptide 34	893	893	D
Peptide 35	910	919	DNTSRYWEPE
Peptide 36	922	928	EAMYTPH

C

Discontinuous B cell epitopes of RdRp

S. No.	RdRp Residue Number	Residue Name	Propensity Score	Discotope Score
1	100	ASP	-1.118	-1.335
2	117	GLN	-3.091	-3.656
3	160	LYS	-3.513	-3.224
4	264	PRO	-2.155	-2.137
5	806	THR	-2.879	-3.008
6	819	LEU	-2.672	-3.63
7	820	VAL	-0.879	-3.538
8	821	LYS	3.032	2.453
9	822	GLN	3.022	0.259
10	823	GLY	1.98	0.027
11	824	ASP	2.13	1.885
12	825	ASP	2.327	1.369
13	826	TYR	1.589	0.371
14	873	PRO	0.749	0.088
15	874	ASN	-0.477	-2.262
16	875	GLN	-3.421	-3.258
17	911	ASN	-0.83	-1.08
18	912	THR	-1.647	-2.147
19	913	SER	-2.016	-1.784
20	919	GLU	-1.995	-2.225
21	922	GLU	-1.367	-2.704
22	923	ALA	-0.296	-1.642
23	926	THR	-1.369	-2.592
24	928	HIS	-0.061	-1.204
25	929	THR	-0.89	-2.168

Figure 3

(i)

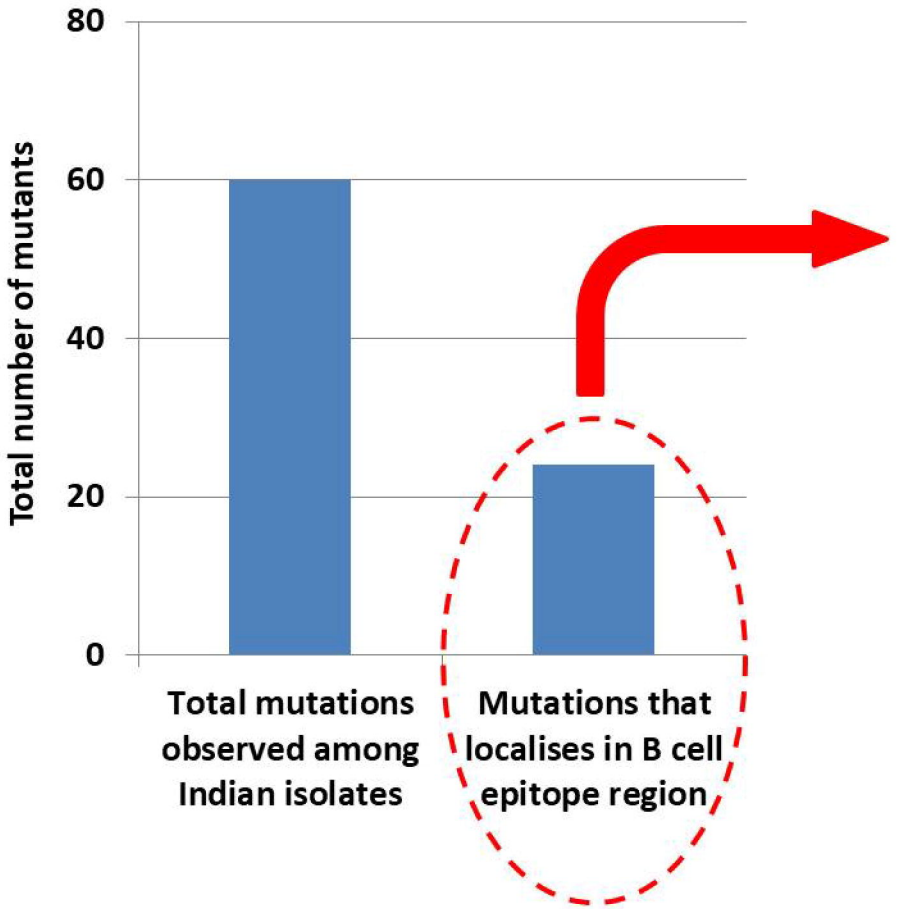

(ii)

S. No.	Mutants	Type of B-cell epitope
1	K59N	Linear-continuous
2	T85I	Linear-continuous
3	K91N	Linear-continuous
4	A95V	Linear-continuous
5	M110K	Linear-continuous
6	D269N	Linear-continuous
7	E278D	Linear-continuous
8	T293I	Linear-continuous
9	H295Y	Linear-continuous
10	P323L	Linear-continuous
11	A406V	Linear-continuous
12	M463I	Linear-continuous
13	I488S	Linear-continuous
14	I536T	Linear-continuous
15	V605A	Linear-continuous
16	M608I	Linear-continuous
17	T644M	Linear-continuous
18	S647I	Linear-continuous
19	Q822H	Discontinuous epitope
20	T848I	Linear-continuous
21	D893Y	Linear-continuous
22	S913L	Linear-continuous
23	S919L	Linear-continuous
24	P925S	Linear-continuous